A Channel Sounding-based Radiation Pattern Measurement Technique for Simultaneous Multi-beam Excitation of Millimeter-Wave Hybrid Beamformer With a Large Antenna Array

Yunsong Gui* [(1)], Tian Hong Loh[(1)], Fabien Heliot[(2)], Mohsen Khalily[(2)], and Rahim Tafazolli[(2)]
(1) National Physical Laboratory, Teddington, Middlesex TW11 0LW, United Kingdom
(2) Institute for Communication Systems, University of Surrey, Guildford GU2 7XS, United Kingdom

Abstract

This paper proposes a novel radiation pattern measurement technique for simultaneous multi-beam excitation characterization of millimeter-wave (mm-wave) hybrid beamforming systems with large antenna arrays based on time-domain channel detection. The method's robustness against interference and the versatility of the hardware platform makes it a good complement to the traditional frequency-domain vector network analyzer (VNA)-based measurement techniques. The proposed approach has been demonstrated and validated via a series of calibration and radiation pattern measurements for single-beam and simultaneous multi-beam excitation test cases.

1. Introduction

Beamforming technologies play an increasingly important role in fifth-generation wireless communication systems and future communication technologies. Especially in recent years, due to the need to solve the frequency band resource bottleneck issue in the sub-6GHz bands, higher frequency bands such as millimeter-wave (mm-wave) have been widely utilized. Compared to the lower frequency band, the sharp beams generated by massive beamforming arrays bring significant gain, making beamforming techniques a mainstream approach to combat the larger path losses due to increased atmospheric absorption at the mm-wave frequencies, which enables long-distance wireless transmission and effectively reduces interference when multiple users share the same time and frequency band resource. However, beamforming gain and associated composite radiation patterns are vulnerable to the many non-ideal factors of the beamforming system, which include inherent defects/limits from the beamforming system and errors from the beamforming weight vector estimation and run-time misfunction of the system.

Traditionally, the frequency-domain vector network analyzer (VNA)-based measurement methods are widely used to evaluate the beamformer with high accuracy. However, there are some disadvantages over such methods. Firstly, there is difficulty in measurement if the antenna array is undetachable to the transceiver. Second, it required a high-precision fully anechoic chamber with enough size to perform a far-field measurement, which makes it hard to evaluate the run-time performance of the beamforming system. Finally, there is an additional difficulty in the measurement cases with multiple beams excited simultaneously. From [1], the composite radiation patterns of multiple beams are independent only if mutual orthogonal beams are simultaneously excited. To tackle the aforementioned problems, in this paper, we present a novel measurement technique based on the time-domain (TD) channel sounding techniques, which have been widely used in measuring the wireless propagation channel [2].

The advantage of the proposed technique lies in its robustness against interference, either from multi-paths or multi-users, which makes it suitable for run-time measurement. Another merit is that its wideband transceiver architecture fully matches with most the transceivers in real-time, which makes it applicable to be used in undetachable antenna array cases. Although in [3], a similar technique is proposed for digital beamformers, this paper explores the technique's capability in hybrid beamformers and presents its advantages by emphasizing its application in calibration and antenna radiation patterns. The paper is organized as follows. Section 2 presents the principles of the TD channel sounding technique applied for hybrid beamformers. Section 3 introduces the Hybrid Beamforming testing facilities. Sections 4 and 5 present the technique's applications in calibration and radiation pattern measurement, respectively, reinforced by real-world measurements. Finally, conclusions are drawn in Section 6.

2. Time domain channel sounding technique for hybrid beamformers

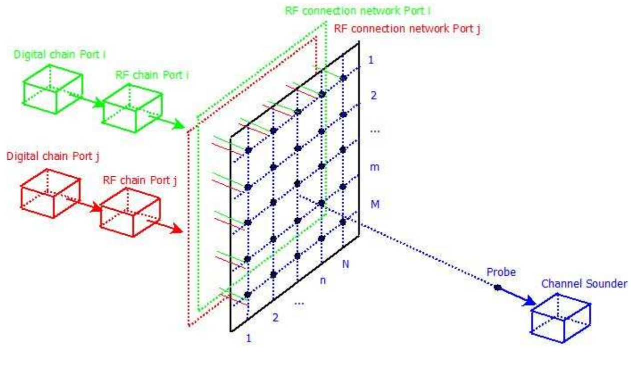

Figure 1. OTA measurement for the hybrid beamformer.

We consider here a measurement scenario as depicted in Figure 1. A typical hybrid beamforming system contains a couple of parallel digital sources and related RF chains, which generate digital and RF signals independently. Depending on the fully or partially connected hybrid beamformer architecture employed, each baseband/RF chain is connected to the entire or part of the antenna array via an RF connection network, which is responsible for routing the incoming RF signal to connected antenna elements. Besides, the connection network is also responsible for adjusting the phase and amplitude of the RF branches according to the configured weight-vector codebook. The receiving probe is used to capture the radiated signal from the beamformer. The received signal $y(t)$ can be represented in the following equation.

$$y(t) = \sum_{i=1}^{I} \{S_i(t) * h_i^{RFchain} * h_i^{OTA}\} * h_P^{RFchain} + n(t) \quad (1).$$

where $S_i(t)$ stands for the signal from ith baseband source, which passes through its connected RF chain $h_i^{RFchain}$ and the i^{th} source associated over-the-air propagation channel response h_i^{OTA} and finally aliases with the signals from other sources at the receiving end. The $h_P^{RFchain}$ is the RF response at receiver side and $n(t)$ is the Additive Gaussian noise (AWGN). The h_i^{OTA} part can be further represented by:

$$h_i^{OTA} = G_{i,C}(\theta_{LoS}) \cdot h_i^{LoS}(t) \cdot \delta(t - \tau_{LoS}) \cdot G_P(\varphi_{LoS}) + \sum_{l=2}^{L} G_{i,C}(\theta_l) \cdot h_i^l(t) \cdot \delta(t - \tau_l) \cdot G_P(\varphi_l) \quad (2).$$

The propagation channel response is characterized by a set of parameter vector $[\tau_l, \theta_l, \varphi_l, h_i^l(t)]$, which represents the wireless channel parameter set of the lth wave, namely relative delay, angle of departure (AoD), angle of arrival (AoA) and complex amplitude. Besides, $G_{i,C}$ and G_P represent the radiation pattern of the beamformer array configured through the weight-vector codebook and the radiation pattern of the receiving probe respectively. In the static propagation channel, the time variation of the channel response can be ignored, and the complex amplitude can be replaced from $h_i^l(t)$ to h_i^l. Whereas in open spaces or in environments with less RF reflection, such as in an anechoic chamber, the line of sight (LoS) path with a parameter vector $[\tau_{Los}, \theta_{Los}, \varphi_{LoS}, h_i^{LoS}]$ usually dominates the receiving signal level, such that (2) can then simply be approximated as

$$\hat{h}_i^{OTA} \approx G_{i,C}(\theta_{LoS}) \cdot h_i^{LoS} \cdot \delta(t - \tau_{LoS}) \cdot G_P(\varphi_{LoS}) \quad (3).$$

Based on these signal equations, we can design a robust channel sounding-based calibration procedure and radiation pattern measurement method for the mm-wave hybrid beamformer system of Figure 1, as it is presented in Figure 2. In the transmission end, the waveform generator creates pseudo-noise (PN) sequences for I parallel sources.

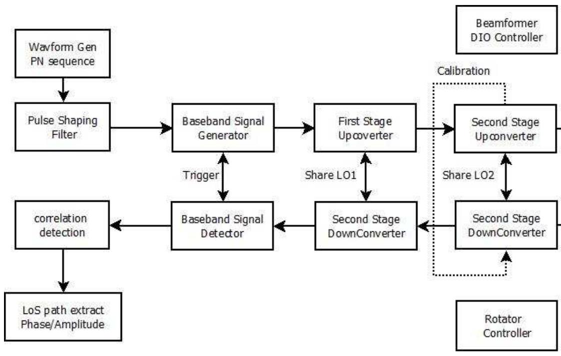

Figure 2. TD channel sounding based measurement process for hybrid beamformers

PN sequence-based waveforms have inherently low autocorrelation and cross-correlation properties, which make them suitable for channel-sounding and multi-user detection. After passing through a pulse shaping filter, the baseband signal is upconverted to mm-wave frequency band via a typical two-stage mixers circuit before it is fed into the mm-wave hybrid beamformer. At the receiving end, the received millimeter wave signal goes through the same process as the transmit wave, but in reverse order, to recover the baseband signal, which is then sampled into a digital sequence $y(n)$. Calibration data for the transmitter-receiver link can be used to cancel the common terms $h_i^{RFchain}$ and $h_P^{RFchain}$ in the (1). A TD correlation detection is applied to obtain the i^{th} source associated channel impulse response $\hat{h}_i^{OTA}$. To estimate the complex amplitude of the LoS path, wideband measurements are required to perform multipath cancellation as the delay resolution is inversely proportional to the signal bandwidth. In addition, super-resolution algorithms [4] can help to distinguish the LoS path from the multipaths within the resolution associated to the measurement bandwidth. The estimate of $\hat{h}_i^{OTA}$in (3) can be useful in at least two distinct manners; namely for measuring the beamformer composite radiation pattern or/and calibrating the beamformer system, which is further discussed in the following sections.

3. Hybrid Beamforming testing facilities

The measurement testbed includes the mm-wave hybrid beamformer and baseband/RF processing system as well as the positioner controller subsystem. The high-performance vector signal transceiver is used with a pair of upconverters and downconverters to form a high-performance mm-wave signal transceiver system. The 3.2 GHz RF signal is upconverted to 26 GHz through mixers and bandpass filters, and a 22.8 GHz local oscillator (LO) signal is imported from a microwave analog signal generator. The LO signal is shared between both RF upconverter channels to ensure the phase coherency. The two RF input signals are routed through a distribution network to each element of the 16-by-8 antenna array, and their phase and envelope can be adjusted. A total 12-bit length Digital Input/Output (DIO) command can ensure the 0.5-dB power resolution and 5.626° phase resolution. A computer is used to configure the beamformer by sending the 16-by-8 weight vector codebook to the Beamformer DIO controller through an ethernet cable, to rotate the Beamformer to the desired direction by sending commands to the rotator controller through the CAN bus connection, and to generate and detect the waveform through its connection with the vector signal transceiver. During the measurement, the beamformer and its DIO controller are placed on a turntable equipped with an azimuth-axis rotator in an anechoic chamber, as shown in Figure 3. A horn antenna, acting as the receiving end probe, is placed at the boresight of the beamformer antenna array where the turntable is set to 0° on the azimuth plane. The setup of the mm-wave hybrid beamforming testbed is depicted in Figure 3. The testbed performance and specification are summarized in Table 1.

4. Beamformer calibration

According to the principle of the composite radiation pattern in a phased array, the composite radiation pattern is determined by the initial coefficient matrix, weight-vector codebook, topology of activated element sets in the phased array, and radiation pattern of each single antenna element, where the initial coefficient includes the initial phase and amplitude of the RF branch of each antenna element. The uncertainties in the initial coefficient matrix of the mm-wave hybrid beamformer play an important role in the distortion of the composite radiation pattern and further contribute to the beam pointing error. Considering the measurement scenario designed for the calibration, the whole set of antenna

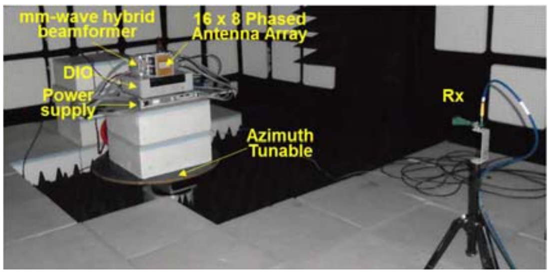

Figure 3. Diagram of the Fully connected hybrid beamforming test environment [5].

Table 1: Hardware specification and performance

Frequency Band	26 GHz
Radio Bandwidth	Up to 1 GHz
Beamformer antenna array	128-element microstrip phased array antenna, 16 × 8
Hybrid architecture	Fully connected
Beam steering angle range	-75° to 75°
Input RF port number	2
Weight vector codebook for each input	Complex (16 × 8) and Logical (16 × 8) Switch On/Off
Phase Tuning Resolution	5.625°
Anechoic chamber size	7 m × 6 m × 6 m
PN sequence size	4096 with 16 repetitions

elements of the hybrid beamformer can be switched on one by one through DIO commands. Accordingly, based on the proposed TD channel sounding method, each channel response $\hat{h}^{OTA}_{i,(m,n)}$ between an active element (e.g. m^{th} in the row and n^{th} in the column) at the transmission end and the probe at the receiving end can be estimated. Since the calibration process aims at aligning all the elements in the phased array and at eliminating the differences of phase and amplitude in the initial coefficient matrix, one of the elements is selected as a reference. Next, the ratio of any element to the reference element is calculated, as follows,

$$\frac{\hat{h}^{OTA}_{i,(m,n)}}{\hat{h}^{OTA}_{i,ref}} = \frac{G_{i,(m,n)}(\theta^{m,n}_{LoS})\cdot h^{LoS}_{i,(m,n)}}{G_{i,ref}\left(\theta^{ref}_{LoS}\right)\cdot h^{LoS}_{i,ref}} = \frac{G_{i,(m,n)}(\theta^{m,n}_{LoS})\cdot e^{j\overrightarrow{d^{m,n}_{ref}}\cdot\overrightarrow{\theta^{m,n}_{LoS}}}}{G_{i,ref}\left(\theta^{ref}_{LoS}\right)} \qquad (4),$$

where the terms $G_P(\varphi_{LoS})$ in (3), which is common to all the links cancels itself out. The term $G_{i,(m,n)}$ is the antenna radiation pattern for element (m,n), which implicates the measurand, initial coefficient matrix.

In Figure 4, the estimated differences of phase and amplitude for all 128 antenna elements are presented. An approximately linear shift in phase over all elements within each row is observed, which is caused by the differences of $h^{LoS}_{i,(m,n)}$ among all antenna elements, determined by the elements' locations in the antenna array, and can be calculated based on sphere wave theory. Finally, after cancelling the differences of h^{LoS}_{i} among all antenna elements, and ignoring the radiation pattern differences between individual elements, the calibration matrix can be obtained to compensate the initial coefficient matrix.

5. Radiation Pattern measurement

For phased antenna arrays, the composite radiation pattern is crucially important to the system performance and also a key indicator for evaluating the beamforming algorithm's performance in some cases. The standard method to

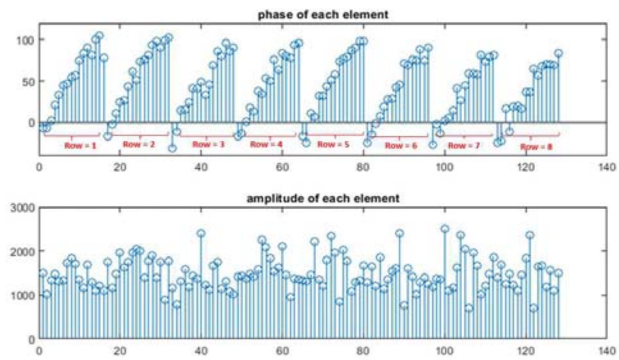

Figure 4 Differences of phase and amplitude in estimates of channel responses for each the antenna element, numbered 0-127

measure composite radiation patterns requires to measure the system response S_{21} in the frequency-domain by using a VNA, which is usually only suitable when one beam is activated. As we can observe from (3), the radiation pattern of the transmitter antenna array $G_{i,c}$ is included in the estimation of the channel response, which can be explored to measure the composite pattern by going through all desired directions of θ_{LoS} via rotating the tuning table. Considering that the other terms in (3) are unchanged during the measurement and by setting the beam peak direction (maximum measured result) as the reference, the normalized composite radiation pattern for the hybrid beamformer antenna array can be formulated as follows:

$$\frac{\hat{h}_{i,\theta_{Azm}}^{OTA}}{\hat{h}_{i,\theta_{peak}}^{OTA}} = \frac{G_{i,composite}(\theta_{Azm})}{G_{i,composite}(\theta_{peak})} \quad (5).$$

It is worth noting that it is still possible to measure the absolute composite radiation pattern as long as the complex channel response h_i^{LoS} and the response of the receiving antenna $G_P(\varphi_{LoS})$ in the fixed incident direction φ_{LoS} have been measured in advanced. The results depicted in Figure 5 are measured for the cases when only one beam is excited, and a series of phase shift weight-vector codebooks are applied to steer the beam pointing to different directions in the azimuth plane. The numbers in the label field represent the directional offset in degrees of the configured beam pointing from the boresight of the BF array. Due to extremely low cross-correlation of the PN sequences, the channel sounding-based method enables the radiation patterns measurement with multi-beam activation, which is difficult to achieve using VNA-based measurement methods. Since activating multiple beams is a common use case in the real world, measurements for multiple activated beams are more valuable than single beam measurements. Consequently, we present in Figure 6 the measurements for the case of two simultaneously activated beams. Two sets of phase shift weight-vector codebooks are applied to the two inputted mm-wave signals respectively, corresponding to the beam pointing directions with azimuth angle of 4 degree and -16 degree from the boresight axis of the hybrid beamformer antenna array. The results in both Figure 5 and Figure 6 show the good agreement with expected beam pointing direction.

6. Summary

This paper presents a novel radiation pattern measurement technique based on time-domain channel sounding approach for simultaneous multi-beam excitation characterization of millimeter-wave hybrid beamformer with large antenna array. Its usefulness has been demonstrated and validated with a series of measurements. The comprehensive evaluation of the proposed approach will be carried out in further work.

7. Acknowledgements

This work was supported in part by the 2021–2025 National Measurement System Programme of the UK Government's Department for Science, Innovation and Technology, Science Theme Reference EMT24, and the EURAMET European Partnership on Metrology (EPM), under 21NRM03 Metrology for Emerging Wireless Standards (MEWS) project (The project 21NRM03 MEWS has received funding from the EPM, co-financed from the European Union's Horizon Europe Research and Innovation Programme and by the Participating States).

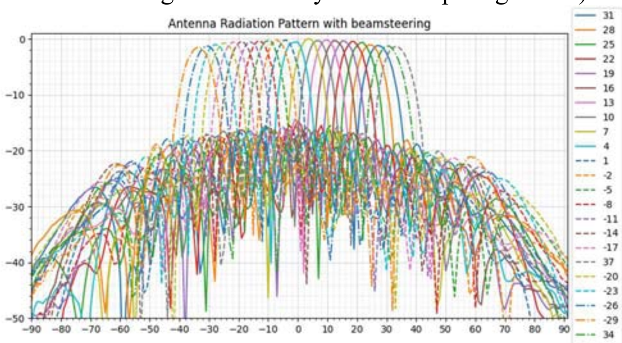

Figure 5. Radiation pattern measurement results for the cases of single beams activation with different directions.

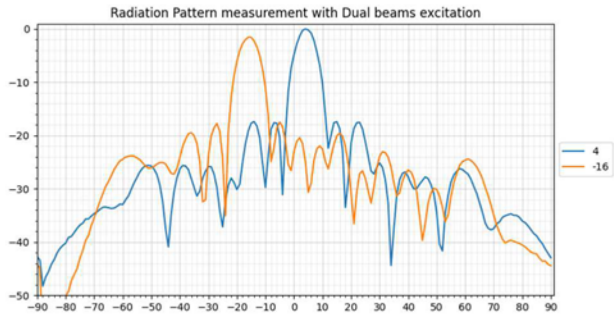

Figure 6. Radiation patterns measurement results for the case of two beams activation.

Funded by the European Union. Views and opinions expressed are however those of the author(s) only and do not necessarily reflect those of the European Union or EURAMET. Neither the European Union nor the granting authority can be held responsible for them.

References

[1] W. White, "Pattern limitations in multiple-beam antennas," IRE Trans. Antennas Propag., **10, 4**, Jul. 1962, pp. 430–436, doi: 10.1109/TAP.1962.1137890.

[2] Y. Yang et al., "Parallel Channel Sounder for MIMO Channel Measurements," IEEE Wireless Communications, **25, 5,** Oct. 2018, pp.16–22, doi: 10.1109/MWC.2018.1800042.

[3] Y. Ji, J. Ø. Nielsen, W. Fan, "A Simultaneous Wideband Calibration for Digital Beamforming Arrays at Short Distances [Measurements Corner]," IEEE Antennas and Propagation Magazine, **63, 3**, Jun. 2021, pp.102–111, doi: 10.1109/MAP.2021.3069244.

[4] B. H. Fleury, M. Tschudin, R. Heddergott, D. Dahlhaus, and K. I. Pedersen, "Channel parameter estimation in mobile radio environments using the SAGE algorithm," IEEE Journal on Selected Areas in Communications, **17, 3**, 1999, pp. 434–450.

[5] S. Payami, et al., "Developing the First mmWave Fully-Connected Hybrid Beamformer with a Large Antenna Array," IEEE Access, **8**, Aug. 2020, pp. 141282 – 141291.